IV International Conference on Computational Methods for Coupled Problems in Science and Engineering
COUPLED PROBLEMS 2011
M. Papadrakakis, E. Oñate and B. Schrefler (Eds)

NUMERICAL ANALYSIS OF CO_2 INJECTION INTO DEFORMABLE SALINE RESERVOIRS: BENCHMARKING AND INITIAL OBSERVATIONS

JOSHUA TARON[*], CHAN-HEE PARK[†], UWE-JENS GÖRKE[*], WENQING WANG[*], OLAF KOLDITZ[*,‡]

[*] Department of Environmental Informatics
Helmholtz Center for Environmental Research - UFZ
Permoserstr. 15, D-04318 Leipzig, Germany
e-mail: joshua.taron@ufz.de, www.ufz.de

[†]Geothermal Resources Department
Korea Institute of Geoscience and Mineral Resources – KIGAM
92 Gwahang-no, Yuseong-gu, Daejeon 305-350, Korea

[‡] University of Technology Dresden, Germany

Key words: Multiphase flow, Deformation, CO_2 Reservoir, Carbon Capture and Storage, Coupled Problems, Hydro-mechanical.

Abstract. A numerical scheme is presented for the solution of coupled multiphase hydro-mechanical problems in deformable porous media. Model verification is conducted against analytical solutions for multiphase flow with capillarity and coupled multiphase hydro-mechanical consolidation. A hybrid monolithic(flow)-staggered(mechanical) numerical solution scheme is verified to be stable for real materials, provided proper error control is placed on the hydraulic to mechanical iteration and the time-stepping scheme. Initial results of CO_2 injection into an aquifer-caprock system do not show significant differences in CO_2 migration rate between flow-only and hydro-mechanical simulations for conservative injection scenarios. However, the results highlight important regions in the reservoir with regard to potential mechanical failure and caprock integrity and suggest the need for further analysis.

1 INTRODUCTION

Long-term storage of CO_2 within deep geological reservoirs, saline aquifers or otherwise, is increasingly cited as a promising method for the global reduction of greenhouse gas emissions. However, the behavior of such reservoirs during CO_2 injection is not well understood in all of the relevant physico-chemical aspects necessary to ensure safe disposal. In addition to complexities associated with modeling individual processes, such as multi-phase hydraulic transport, chemical dissolution and transport, or mechanical deformation, the interaction between such processes is often complex and non-linear.

Being less dense than water, supercritical CO_2 requires an impermeable seal (caprock) above the target reservoir to prevent escape to the surface. Over the vast areas that injected CO_2 will migrate during long term injection, potentially greater than 100 km^2 for a 1000-MW coal-fired power plant injecting over 30 years into a 100m thick reservoir [1], the caprock is extremely unlikely to exhibit homogeneity or a lack of potential escape conduits such as faults or large fracture zones.

Beyond uncertainty in initial state, the aquifer-caprock system will be prone to dynamic alteration in permeability and porosity resulting from hydraulic and thermal stimulation. Mechanical failure will be an important consideration where elevated shear stresses are likely, such as at boundaries of materials with strongly different properties (such as the reservoir caprock interface), and such failure has direct consequences on the integrity of the system.

This paper will be one in a series of which examine development and application of a large scale numerical model (OpenGeoSys, [2]) for analysis of these situations. To have sufficient confidence in the ability of a numerical model to answer these very complex questions, it is first necessary to build confidence in the model in more fundamental respects. In this paper we focus on model verification for coupled multi-phase hydromechanical (H2M) problems. Several benchmarks test the individual and combined processes against analytical accuracy. Stability is discussed in relation to time-stepping schemes and inter-process coupling tolerance. A simple reservoir-caprock system is examined to highlight some important differences between typical multi-phase flow simulations and those that include contribution from mechanical deformation and also to examine mechanical integrity of the storage system.

2 GOVERNING EQUATIONS

The governing field equations for modeling multiphase flow in deformable porous media are formulated based on local mass and momentum balance relations of the constituents. The general mass balance of a component, κ, may be written (neglecting diffusive/dispersive flux),

$$\frac{\partial\left(\phi S_\kappa \rho_\kappa\right)}{\partial t} + \nabla \cdot \left(\phi S_\kappa \rho_\kappa \mathbf{v}_\kappa\right) = 0\,, \tag{1}$$

in terms of the porosity, ϕ, saturation, S_κ, density, ρ_κ, and phase velocity, $\mathbf{v}_\kappa$. Expanding the time derivative term and utilizing the material time derivative of a component relative to the motion of the deformable solid,

$$\frac{d}{d^s t} = \frac{\partial}{\partial t} + \mathbf{v}_s \cdot \nabla\,, \tag{2}$$

introduces the relationship,

$$\phi \frac{d\left(S_\kappa \rho_\kappa\right)}{d^s t} + S_\kappa \rho_\kappa \frac{d\phi}{d^s t} + \phi S_\kappa \rho_\kappa \nabla \cdot \mathbf{v}_s + \nabla \cdot q_\kappa^r = 0\,, \tag{3}$$

where the flux, q_κ^r, is relative to solid motion. The Lagrangian form (utilizing Eq. (2)) of solid mass balance is,

$$\frac{d\left(1-\phi\right)\rho_s}{d^s t}+\left(1-\phi\right)\rho_s\nabla\cdot\mathbf{v}_s=0\,, \tag{4}$$

from which the expanded storage term yields the porosity derivative [3],

$$\frac{d\phi}{d^s t}=\frac{\left(1-\phi\right)}{\rho_s}\frac{d\rho_s}{d^s t}+\left(1-\phi\right)\nabla\cdot\mathbf{v}_s\,. \tag{5}$$

Substituting this into Eq. (3) yields,

$$\phi\frac{d\left(S_\kappa\rho_\kappa\right)}{d^s t}+S_\kappa\rho_\kappa\left[\nabla\cdot\mathbf{v}_s+\frac{\left(1-\phi\right)}{\rho_s}\frac{d\rho_s}{d^s t}\right]=-\nabla\cdot q_\kappa^r\,, \tag{6}$$

where an assumption of small strain negates the resulting two terms: $\mathbf{v}_s\cdot\nabla S_\kappa\rho_\kappa$ and $\mathbf{v}_s\cdot\nabla\rho_s$. A Biot formulation is utilized to represent the solid density time derivative [cf. 4] and Eq. (6) is divided into two fluids; a wetting fluid (subscript *w*) and a non-wetting fluid (subscript *nw*). Algebraic manipulations target three primary variables for the numerical solution; wetting fluid pressure, P_w, non-wetting fluid saturation, S_{nw}, and the solid displacement vector, **u**:

$$S_w\left[\frac{\phi}{K_w}+\frac{\alpha-\phi}{K_g}\right]\frac{dP_w}{d^s t}-\phi\frac{dS_{nw}}{d^s t}+\alpha S_w\nabla\cdot\frac{d\mathbf{u}}{d^s t}=-\nabla\cdot\left[\frac{\mathbf{k}k_w^r}{\mu_w}\left(-\nabla P_w+\rho_w\mathbf{g}\right)\right] \tag{7}$$

and

$$\begin{aligned}&S_{nw}\left[\frac{\phi}{K_{nw}}+\frac{\alpha-\phi}{K_g}\right]\frac{dP_w}{d^s t}+\phi\left[1-\frac{S_{nw}}{K_{nw}}\frac{dP_c}{dS_w}\right]\frac{dS_{nw}}{d^s t}+\\&\alpha S_{nw}\nabla\cdot\frac{d\mathbf{u}}{d^s t}=-\nabla\cdot\left[\frac{\mathbf{k}k_{nw}^r}{\mu_{nw}}\left(-\nabla P_w-\frac{dP_c}{dS_w}\nabla S_{nw}+\rho_{nw}\mathbf{g}\right)\right]\end{aligned}\,. \tag{8}$$

Relative fluid flux (the right hand side term) is obtained from Darcy's law. The solid displacement derivative is $d\mathbf{u}/d^s t=\mathbf{v}_s$, and variables are the intrinsic permeability tensor, **k**, viscosity, μ_κ, fluid density, ρ_κ, gravity vector, **g**, solid *grain* modulus, K_g, and Biot's alpha $\alpha\approx 1-K/K_g$, where K is the solid bulk modulus. Fluid pressure is related to the capillary pressure, P_c, as $P_w+P_c=P_{nw}$. The bulk modulus, K_κ, is, by definition,

$$1/K_\kappa\equiv\frac{1}{\rho_\kappa}\frac{\partial\rho_\kappa}{\partial p_\kappa}\bigg|_{\partial T/\partial t=0}\,. \tag{9}$$

The third governing equation (for the H2M problem) is given by linear momentum balance on the solid mixture (stress equilibrium equation),

$$\nabla\cdot\left(\boldsymbol{\sigma}-\bar{P}\mathbf{I}\right)+\rho_m\mathbf{g}=0\,, \tag{10}$$

for the total stress tensor, $\boldsymbol{\sigma}$, with an appropriate stress/strain constitutive relationship, $\boldsymbol{\sigma} = \mathbf{D}\boldsymbol{\varepsilon}$, in terms of the strain tensor $\boldsymbol{\varepsilon} = \frac{1}{2}\left(\nabla \mathbf{u} + \left(\nabla \mathbf{u}\right)^T\right)$. Effective fluid pressure is defined as $\overline{P} = S_w P_w + S_{nw} P_{nw}$ and the mixture density is $\rho_m = \phi\left(S_w \rho_w + S_{nw} \rho_{nw}\right) + \left(1-\phi\right)\rho_s$. Equations (7) and (8) are solved globally, with an iterative coupling to Eq. (10). Alternate assumptions are sometimes used for the mean fluid pressure, such as the perfect wetting fluid assumption (all grains are at all times perfectly wetted by the wetting fluid), $\overline{P} = P_w$.

2.1 Saturation equations

Relative permeability and capillary pressure are defined utilizing the Brooks-Corey relationship. For the effective saturation, $S_e = \left(S_w - S_w^r\right) \Big/ \left(1.0 - S_w^r - S_{nw}^r\right)$, these relationships are:

$$\begin{aligned} k_w^r &= S_e^{3+2/m} \\ k_{nw}^r &= \left(1-S_e\right)^2 \left(1-S_e^{1+2/m}\right), \\ P_c &= P_b S_e^{-1/m} \end{aligned} \tag{11}$$

for the entry pressure, P_b, and the residual saturations, S_κ^r.

3 NUMERICAL METHOD

Simulations utilize the open source numerical simulator OpenGeoSys (OGS) [2], in continued development by the authors. Weak formulations of the above governing equations (Eqs. (7), (8), and (10)) are derived using the method of weighted residuals. A standard Galerkin procedure is followed, multiplying the equations by arbitrary test functions and integrating over the domain of interest. Time discretization is designed as a generalized first order difference scheme, but all simulations in this paper utilize a fully implicit Euler scheme. The fluid equations (7 and 8) are solved globally in a single matrix, for a resulting non-linear system that is iterated with a Picard linearization. Coupling to the solid equation (and vice versa) is performed with an iterative linking of this global equation (7 and 8) to that of the solid (10). Iteration is performed until a tolerance is met that defines stabilization of error between the solid and fluid system. Such an error tolerance is also a reasonable foundation to build an adaptive time stepping scheme. This is briefly discussed in the following section.

3.1 Tolerance and stability

Convergence of the iteration between the solid and fluid system can depend on error reduction in any of the three primary variables, and potentially a third: the capillary pressure. As the fluid scheme utilizes saturation as a primary variable, the 0 to 1 bounds introduce potential instability in the system. As wetting saturation falls to near the wetting residual saturation, the non-linear relationship to P_c generates a rapid increase in P_c, and thus a rapid mean pressure response. Therefore, iteration and/or time stepping based on P_w and S_{nw} are inadequate in this case, as they will not recognize the rapid system change. We find the most stable method to define error and time stability in the fully H2M system to be that of the mean

pressure. Therefore, both H2 $\leftrightarrow$ M coupling and adaptive time stepping can be stably confined by controlling equilibration of the mean pressure, $\overline{P} = P_w S_w + P_{nw} S_{nw} = P_w + P_c S_{nw}$.

The semi-staggered solution also has potential stability issues dependent upon material properties. When the fluid becomes highly incompressible relative to the solid (stiff system) the solution will fail. This is best defined relative to the Skempton coefficient, B (Table 1), a lower value of B ensures greater stability and we have observed that this criterion is generally independent of loading rate. The Skempton coefficient, $B = -d\overline{P} / d\sigma_m \big|_{\zeta=0}$ is, in fact, a perfect criterion, as it is a direct measure of strength of coupling between the solid and fluid system. In fact, in undrained coupling methodologies (cf. [5]), this *is* the coupling linkage between Eqs. (7-8) and (10). In 1-D, as in the analytical solution below, it is the 1-D Skempton coefficient, B_v, that measures strength of coupling and thus stability.

For real systems, where fluids and solid grains are compressible, we have experienced no trouble. It is the introduction of incompressible fluids that tend to cause instability. It is none-the-less important for a given problem and set of solid/fluid properties to examine stability with appropriate benchmarks (as provided below) before extending to the full system.

4 MODEL VERIFICATION

4.1 Two-phase flow

Validation of the flow component is provided by a 1-D solution to the incompressible fluid mass balance equation [6, 7],

$$\phi\left(1 - S_w^r - S_{nw}^r\right)\frac{\partial S_\kappa}{\partial t} = -q_\kappa\left(t,0\right)\frac{\partial f_\kappa\left(S_w\right)}{\partial x} + \frac{\partial}{\partial x}\left(D_\kappa\left(S_w\right)\frac{\partial S_\kappa}{\partial x}\right) \tag{12}$$

where f_κ is a fractional flow function,

$$f_\kappa\left(S_w\right) = \frac{\lambda_\kappa\left(S_w\right)}{\lambda_w\left(S_w\right) + \lambda_{nw}\left(S_w\right)} \tag{13}$$

for the mobility, $\lambda_\kappa = k_\kappa^r / \mu_\kappa$. And D_κ is a diffusivity function ($D_{nw} = -D_w$),

$$D_w\left(S_w\right) = \frac{\lambda_w\left(S_w\right)\lambda_{nw}\left(S_w\right)}{\lambda_w\left(S_w\right) + \lambda_{nw}\left(S_w\right)}\frac{dP_c}{dS_w}. \tag{14}$$

and where the source term is required to take the form $q_\kappa\left(t,0\right) = At^{-1/2}$ for $A > 0$. McWhorter and Sunada [7] provided the first analytical solution to this relationship, and a nicely modified improved form was presented by [6]. It is this modified form that we utilize in our comparison. See [6] for the semi-analytical methodology required to generate the solution. A 1-D flow problem is set up with an initially high wetting saturation prescribed in the domain. A source injection of non-wetting fluid, $q_\kappa\left(t,0\right)$, is applied to the leftmost inlet and saturation monitored in time. The results are provided in Figure 1. It is quite difficult to represent the sharp front dictated by the analytical solution, which would require a very tight spatial discretization. None-the-less, the solution is quite agreeable.

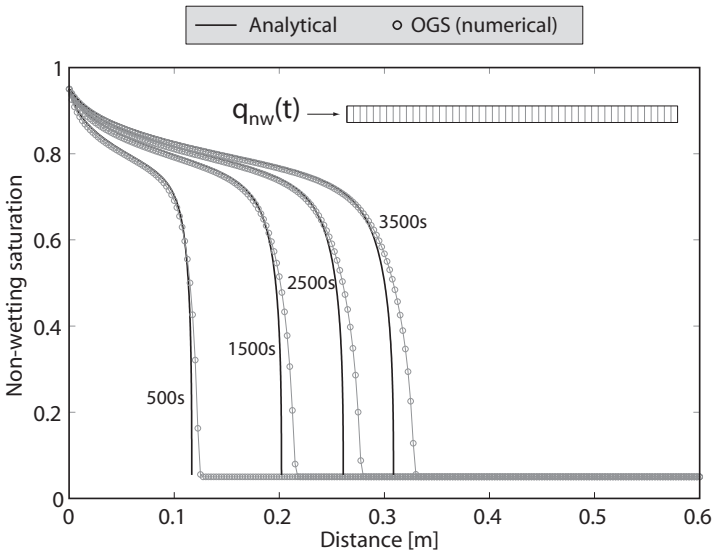

Figure 1. Saturation profiles for the numerical and analytical solutions of the 1-D two-phase flow problem.

Note: A simpler analytical solution is available if $P_c = 0 = \text{constant}$ is prescribed (Buckley-Leverett equation), but a solution that considers P_c variation is strongly desirable for code validation. Furthermore, because the dP_c / dS_w term vanishes in Eq. (8), and this term represents a stabilizing diffusive term in the relationship (see Eq. (14)), we cannot achieve a stable solution to the $P_c = 0$ problem without an upwinding scheme. An upwinding scheme was implemented for this purpose and achieved accurate reproduction of the $P_c = 0$ analytical solution, but those results are not presented here. All results shown in this paper do *not* utilize an upwinding scheme.

4.2 H2M coupling

In this section we test the fundamental premise and validity of a coupling between fluid flow and mechanical deformation. Mechanical compression generates a fluid pressure response, while pressure storage and dissipation affects the mechanical condition via the effective stress. Terzaghi has provided the framework to test such a problem.

This problem tests the fundamental linkage within a hydro-mechanical coupling. It is a convenient test of both the deformation and flow modules but most importantly guarantees that the coupling is correct between them. Without it, H2M (or HM) coupling does not exist. It is necessary for this benchmark to define the composite fluid bulk modulus,

$$\frac{1}{K_f} = \frac{S_w}{K_w} + \frac{S_{nw}}{K_{nw}} . \tag{15}$$

This relationship is accurate for immiscible (or slowly miscible) fluids without penetrating bubbles and allows us provide an analytical solution for H2M where none would otherwise be available.

Table 1. Poroelastic quantities (see [8, 9]).

Parameter	Description	Equation
B	Skempton coefficient	$\frac{\alpha}{\left[\alpha-\phi(1-\alpha)\right]+\phi\frac{K}{K_f}}$
K^u	Undrained bulk modulus	$\frac{K}{1.0-\alpha B}$
G	Shear modulus	$3K\frac{1-2\nu}{2+2\nu}$
ν^u	Undrained Poisson's ratio	$\frac{3K^u-2G}{2\left(3K^u+G\right)}$
B_v	Uniaxial Skempton coefficient	$\frac{B}{3}\frac{1+\nu_u}{1-\nu_u}$
K_v	Uniaxial bulk modulus	$3K\frac{(1-\nu)}{1+\nu}$
K_v^u	Uniaxial undrained bulk modulus	$3K^u\frac{\left(1-\nu^u\right)}{1+\nu^u}$
S_v	Uniaxial storage	$\frac{\alpha}{K_v B_v}$

4.2.1 Analytical solution

For a single fluid phase, the analytical solution for pressure dissipation and solid deformation in time are available. The analytical solution to this problem has been utilized a number of times for this very purpose. Beginning from the 1-D fluid diffusion equation of hydrogeology,

$$\frac{\partial \overline{P}}{\partial t}-c\frac{\partial^2 \overline{P}}{\partial z^2}=0 \tag{16}$$

where c is 1-D fluid diffusivity. The pore pressure response to a vertical load, σ_z, applied linearly over time ($\sigma_z^{t=0^-}=0$) to the top of the column at a rate, $\dot{\sigma}_z=d\sigma_z/dt$, is, [10, Eq. 6.50],

$$\overline{P}\left(z,t\right)=P_0\left\{1.0-\left(\frac{L-z}{L}\right)^2-\frac{32}{\pi^3}\left[\sum_{m=0}^{\infty}\frac{\left(-1\right)^m}{\left(2m+1\right)^3}\exp\left[-\lambda^2 ct\right]\cos\left[\lambda\left(L-z\right)\right]\right]\right\}, \tag{17}$$

where the total pressure generation is

$$P_0=\frac{L^2}{2c}\left(B_v\dot{\sigma}_z\right), \tag{18}$$

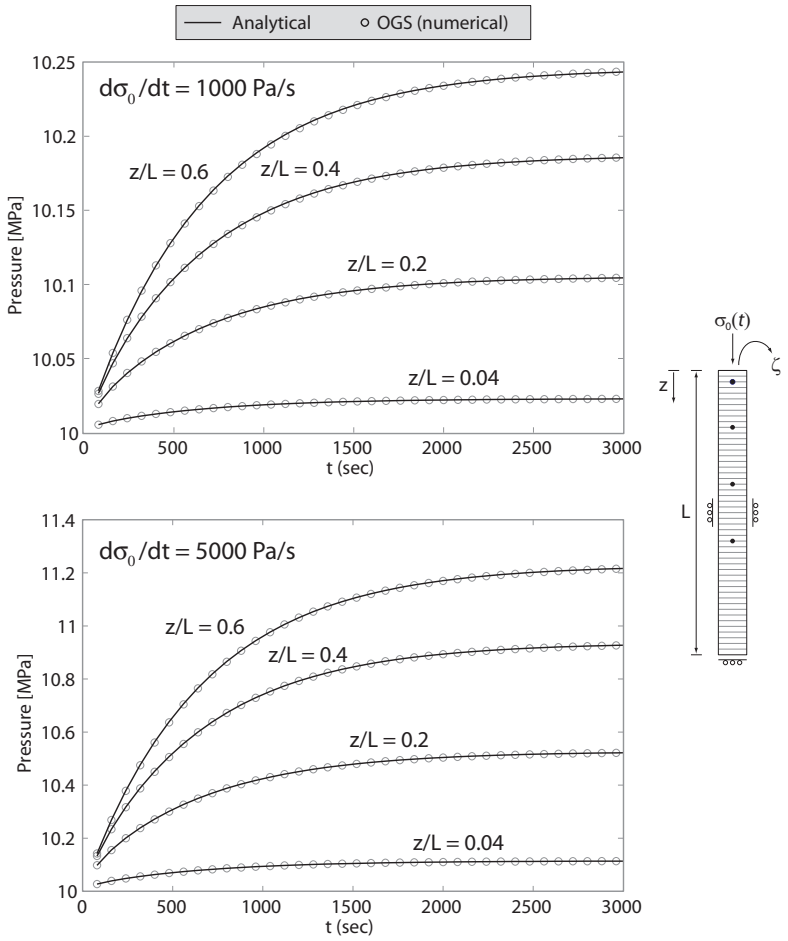

Figure 2. Numerical and analytical solutions of the coupled H2M Terzaghi consolidation problem with variable loading rate.

for the factor, $\lambda = (2m+1)\pi/(2L)$, the total column length, L, and the location in the column (downward from the applied stress), z. The 1-D Skempton coefficient,

$$B_v = -\left.\frac{d\bar{P}}{d\sigma_{zz}}\right|_{\varepsilon_{xx}=\varepsilon_{yy}=\zeta=0} = \frac{\alpha}{K_v S_v}, \tag{19}$$

is given purely by micromechanical, poroelastic considerations from the uniaxial drained bulk modulus, K_v, and the 1-D specific storage, S_v (Table 1). The 1-D diffusivity is also a derivative of the 1-D storage:

$$c = \frac{k}{\mu S_v}, \tag{20}$$

If utilizing an applied step load at time $t = 0^+$ an analytical solution is available for pressure and displacement. For this validation, only the linear loading rate solution is examined. Because displacement is the primary variable in the FEM formulation, the

displacement must be accurate in order to generate the correct pressure response: we find no need to reproduce the results of a step load analysis here.

The domain is given the initial properties, $S_w = 0.8$, $k_w^r = k_{nw}^r = 0.5$, and $K_w = 2.93\,\text{GPa}$ and $K_{nw} = 1.19\,\text{GPa}$. Capillary pressure is set constant at zero and relative permeability is constant. Utilizing Eq. (15) the appropriate coefficient (Eq. (19)) for calculation of the analytical solution (Eq. (17)) can be obtained. Two loading rates ($\dot{\sigma}_z = d\sigma_z / dt$) are examined in Figure 2 and adaptive time stepping and iteration tolerance control is utilized as discussed in section 3.1.

5 TEST CASE: AQUIFER CAPROCK SYSTEM

This section presents a few initial results of H2M flow in a simple aquifer-caprock system. Figure 3 illustrates the geometry and boundary conditions. A depth of 2000m is chosen, and fluid properties of water and CO_2 assigned appropriately. A vertical stress of 44MPa is applied at the upper boundary and an initial fluid pressure assigned to the total domain at 20MPa. CO_2 is injected centrally to the reservoir, at the maximum non-wetting saturation and injection pressure is constant, conservatively, at 22MPa. East and west boundaries constrain zero horizontal displacement, and so the vertical and horizontal stress state is allowed to develop naturally. Real reservoirs will exhibit a greater degree of initial instability due to tectonic stress states.

The aquifer is given mechanical parameters of generic sandstone, and the caprock modified slightly from this in terms of saturation dependent properties. Mechanical properties are not altered from reservoir values for the caprock, which generates a more stable physical situation. Introducing a boundary of differing mechanical properties would decrease the mechanical stability beyond that observed in Figure 4. Property values are shown in Table 2. Stability of the reservoir is indexed to a "factor of safety (f_s^s)" defined by a Mohr-Coulomb failure criterion. In 2-D, the criterion states that mechanical failure is favorable when the current maximum shear stress, $\tau_m = 1/2\left(\sigma_1 - \sigma_3\right)$, becomes [11],

$$\left|\tau_m\right| \geq C_h \cos\varphi + \left(\sigma_m - \bar{P}\right)\sin\varphi, \tag{21}$$

where σ_1 and σ_3 are the maximum and minimum principle stresses, respectively, and $\sigma_m = 1/2\left(\sigma_1 + \sigma_3\right)$ is the mean normal stress. A relationship is presented based on Eq. (21) that defines a "factor of safety (f_s^s)" for shear slip/failure along an optimally oriented failure plane,

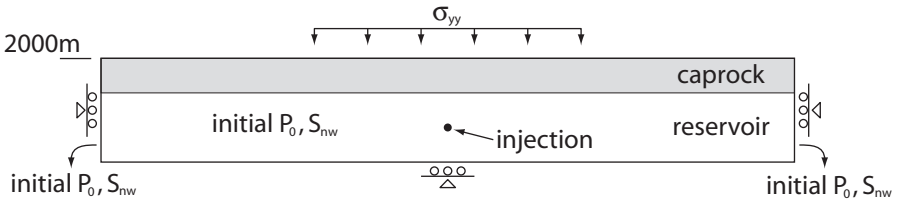

Figure 3. Geometry of reservoir system.

Table 2. Parameter values for reservoir simulation.

Parameter	Reservoir	Caprock
S_{lr}	0.30	0.30
S_{gr}	0.02	0.02
P_b	19.6kPa	3100kPa
k	1.9×10^{-13} m^2	1.9×10^{-17} m^2
ϕ	0.19	0.02
Young's Modulus	14.4 GPa	14.4 GPa
Poisson Ratio	0.2	0.2
α	0.8	0.8

$$f_s^s = \frac{|\tau_m|}{C_h \cos\varphi + (\sigma_m - \bar{P})\sin\varphi}, \tag{22}$$

for the cohesion, C_h = 50MPa, and friction coefficient, $\tan\varphi = 0.6$. Values of $f_s^s \geq 1$ imply incipient failure. Results of this criterion are presented in Figure 4 (left) for two values of cohesion. The lower value (5MPa) represents the case where optimally oriented, pre-existing fractures are present. The factor of safety is not violated in either case. However, the physical description utilized here is extremely conservative with respect to initial reservoir stability, discontinuity of mechanical properties across layers, and the injection pressure. Regardless, prime locations for reservoir instability are easily discernable. With lower cohesion, a greater fraction of the caprock is in the higher range of f_s^s and the magnitude of the instability is also higher (the latter is of course expected). It is clear that the highest risk of failure is at the reservoir/caprock interface near the injection region (a result in agreement with the study of [12]), not necessarily good news given the importance of caprock integrity. Additionally, although not strongly observable in the figures due to the domination of the material interface, a region of increased instability can be observed to follow the advance of the CO_2 migration front. Whether or not this will be an important observation is the focus of future study.

Figure 4 (right) illustrates the difference in CO_2 migration between H2M and H2 simulations. While some small difference is visible, it is not significant in this case. However, as porosity and permeability are not allowed to change in these simulations, the difference was not expected to be large. Permeability was shown to increase by nearly 50% in the CO_2 injection study of [12]. Furthermore, the introduction of thermal effects, shown to have dire consequences on permeability in geothermal reservoirs ([13]), may be important in this regard. This, also, will be included in future work.

6 CONCLUSIONS

A numerical scheme has been implemented for the coupled solution of multiphase flow and mechanical deformation during the injection of CO_2 into geological reservoirs. Benchmarking of the multiphase hydraulic and also the multiphase hydro-mechanical coupling has been conducted against analytical solutions. Results are accurate for the fundamental coupling methodology.

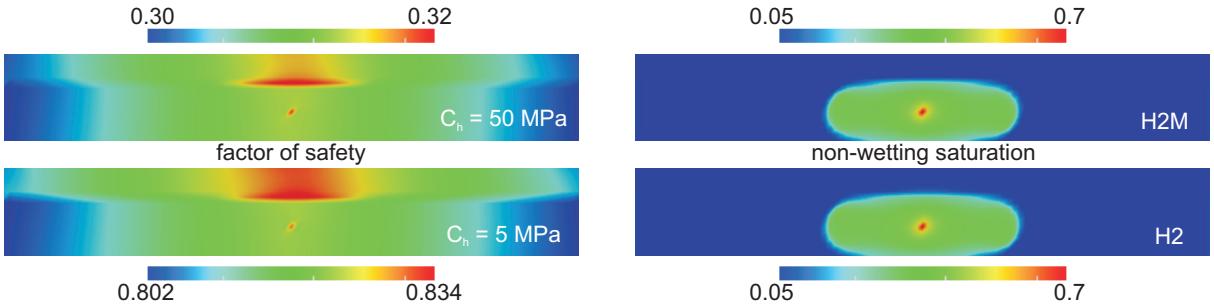

Figure 4. Left: Factor of safety (Top: C_h = 50MPa Bottom: C_h = 5MPa) and Right: CO_2 saturation (Top: H2M simulation Bottom: H2 simulation) for alternate test conditions.

Initial results for a simplified aquifer-caprock system do not show significant differences between H2 and H2M simulations for the very conservative injection scenario utilized here. More importantly, however, the coupled problem allows examination of reservoir integrity and the potential for breaching of an intact caprock. The interface between zones of different material properties (such as between the reservoir and caprock) are particular targets for mechanical failure, and improper selection of injections rates could easily lead to a breach of trapping integrity. More complex stress states will be important for a more detailed analysis in addition to sensitivity analysis of injection scenarios.

Future work will seek greater complexity in geometric representation of the reservoir system. Principally, the introduction of high permeability zones within the caprock and extension of the geometry to include additional geological layers. Greater complexity will be sought with regard to constitutive relationships defining how porosity and permeability will be altered dynamically within the system.

6 ACKNOWLEDGEMENTS

This study is the result of partial funding from the German Federal Ministry of Education and Research (BMBF) as part of joint projects in the framework of the Special Programme GEOTECHNOLOGIEN and from the Helmholtz Association within the Research Programme “Renewable Energies – Geothermal Technologies”.

REFERENCES

[1] Pruess K, Xu T, Apps J, et al. Numerical modeling of aquifer disposal of CO_2. Society of Petroleum Engineers (SPE), Paper number 66537 2001.

[2] Wang W, Kosakowski G, and Kolditz O. A parallel finite element scheme for thermo-hydro-mechanical (THM) coupled problems in porous media. Computational Geosciences 2009;35:1631-1641.

[3] Bear J and Bachmat Y. Introduction to modeling of transport phenomena in porous media. Netherlands: Kluwer Academic; 1991,553.

[4] Lewis RW and Schrefler BA. The finite element method in the static and dynamic deformation and consolidation of porous media, 2nd ed. West Sussex, England: John Wiley & Sons; 1998,492.

[5] Taron J, Elsworth D, and Min KB. Numerical simulation of thermal-hydrologic-mechanical-chemical processes in deformable, fractured porous media. Int J Rock Mech Min Sci 2009;46(5):842-854.

[6] Fucik R, Mikyska J, Benes M, et al. An improved semi-analytical solution for verification of numerical models of two-phase flow in porous media. Vadose Zone Journal 2007;6:93-104.

[7] McWhorter DB and Sunada DK. Exact integral solutions for two-phase flow. Water Resour Res 1990;26(3):399-413.

[8] Detournay E and Cheng AH-D, Fundamentals of poroelasticity, In: J.A. Hudson, Editor. Comprehensive rock engineering. New York: Pergamon; 1993.

[9] Wang HF. Theory of linear poroelasticity. Princeton: Princeton University Press; 2000.

[10] Wang HF. Theory of linear poroelasticity. Princeton: Princeton University Press; 2000,287.

[11] Jaeger JC, Cook NGW, and Zimmerman RW. Fundamentals of rock mechanics, 4th ed. Malden, MA: Blackwell Publishing; 2007.

[12] Rutqvist J and Tsang C-F. A study of caprock hydromechanical changes associated with CO_2 injection into a brine formation. Environ Geol 2002;42:296-305.

[13] Taron J and Elsworth D. Thermal-hydrologic-mechanical-chemical processes in the evolution of engineered geothermal reservoirs. Int J Rock Mech Min Sci 2009;46(5):855-864.